Surface Resistance to Permeation through the Silicalite Single Crystal Membrane: Variation with Permeant

M. Goktug Ahunbay and J. Richard Elliott, Jr.*

Chemical Engineering Department, The University of Akron, Akron, Ohio 44325-3609

Orhan Talu

Chemical Engineering Department, Cleveland State University, Cleveland, Ohio 44115-2425

Received: January 7, 2004; In Final Form: April 7, 2004

The variation of surface resistances to diffusion of molecules through the silicalite single-crystal membranes as a function of permeants has been investigated using the Dual Control Volume-Grand Canonical Molecular Dynamics method. For this purpose three spherical molecules, CH_4, Ar, and CF_4, have been selected. This selection enabled the study of a range of molecular diameters and interaction energies. Simulation results showed that the magnitude of surface resistance in zeolite membranes depends on the permeant-crystal interaction size and energy. Furthermore, the *range* of the surface resistance, defined as the distance from the surface beyond which the surface resistance becomes constant, is primarily a function of molecular size: For smaller molecules the range of surface resistances is shorter while its magnitude is lower. Variations in mass-transfer resistances and diffusivities were studied in further detail with a parametric sensitivity analysis by varying permeant-crystal interaction size and well depth, as well as molecular weight in the manner of a factorial design. This procedure allowed checking for the significance of these factors and their cross-interactions during adsorption from the gas phase into the silicalite. The parametric study showed that the Lennard-Jones gas-crystal size interaction dominates the surface resistance of molecules that penetrate silicalite crystals, but interaction energy is also significant. Although, different sets of parameters yield similar equilibrium concentration values in adsorption studies, the surface resistance varies drastically with variations in these parameters.

1. Introduction

Zeolite membranes have attracted considerable interest in recent years, as they combine the general advantages of inorganic membranes (thermal stability, solvent resistance) with shape selectivity, making them versatile adsorbents and specific catalysts. Applications of adsorption cover a wide range of processes from bulk gas separations to purification. Both equilibrium and dynamics impact the adsorption process. Whereas the equilibrium data in the literature are consistent, the dynamic data, that is, diffusivities, show variations of several orders of magnitude depending on the experimental methods. Typical experimental methods include batch uptake measurements as in a gravimetric method,[1] and flow methods such as fixed-bed responses to pulse and step changes.[2] Karger and Ruthven[3,4] suggested several possible reasons for this discrepancy: different ranges of applicability of macroscopic and microscopic methods, different methods of crystal synthesis, different procedure of sample regeneration, and the presence of other extraneous mass and heat transfer resistances. The discrepancy between microscopic and macroscopic perspectives may also be explained in part by the relative contribution of intracrystalline and intercrystalline diffusion. Surface resistances exist at the pore entrances and exits due to the discontinuity in the crystal potential field.[5,6] At the continuum scale, Kocirik and co-workers[5] argued that surface resistance can exceed intracrystalline resistance by several orders of magnitude for crystals smaller than 1 μm. Barrer[7] and Karger[8] developed generalized flux expressions that account for the "evaporation barrier" that arises due to the steep change in potential energy at the zeolite surface.

The single-crystal membrane (SCM) method,[9,10] is based on the direct measurement of diffusive flux through the zeolite at transient and steady state conditions and allows bridging of techniques between the microscopic and macroscopic because it is absent of inter-crystalline resistances. Entrance and exit barriers are the only existing surface-resistance types in the case of SCM, since the membrane is formed by a single massive zeolite crystal. Therefore, there are only three contributions that comprise the diffusion process of a gas molecule through the SCM: entrance to the pores (adsorption), intracrystalline diffusion, and exit from the pores (desorption). Several researchers, such as Maginn et al.,[11] Ford and Heffelfinger,[12] Nicholas et al.,[13] and Hernandez and Catlow[14] investigated the intracrystalline diffusion of hydrocarbon sorbates inside the zeolite crystal via molecular simulations. Their simulation studies yielded diffusion-coefficient values in agreement with Quasi-elastic Neutron Scattering (QENS) and Pulsed-Field Gradient Nuclear Magnetic Resonance (PFG-NMR) methods.[3,4]

Entrance into zeolites has been studied by a number of authors.[6,15,16] They investigated the trajectories of gas atoms passing through the outer surface of the crystal. Their simulation studies showed that entrance into the pore was limited by the ease with which the molecule fit into a pore given its size and conformation. Vigné-Maeder et al.[15] further concluded that the size effects of the permeating molecules were not sufficient to

* To whom correspondence should be addressed. E-mail: jelliott@uakron.edu.

10.1021/jp040002w CCC: $27.50
Published on Web 05/18/2004

explain the resistance at the surface of the zeolite crystal during the study of diffusion of Ar and Xe molecules.

Arya et al.[17] studied the limiting effect of the pore exit on the transport rate of methane molecules in AlPO4−5-type zeolite. Their study showed that the surface barrier decreases with temperature, and increases at sorbate loadings lower than 0.5 molecules per unit cell where the escape of a molecule is unaffected by the presence of the other molecules. At higher sorbate loadings, the local clustering of molecules results in a significant reduction of the pore exit barrier.

The recent work of Bowen et al.[20] compared the experimental and theoretical results for pure component permeance through a supported silicalite membrane. They pointed out that total flux through a polycrystalline membrane includes contributions from flow through both zeolitic (intracrystalline) and nonzeolitic pores that separate zeolite crystals. Their study aimed to isolate the zeolitic diffusion in order to model polycrystalline membranes in combination with a reasonable description of gas permeation through the nonzeolitic pores.

The importance of mass-transfer resistance to diffusion at interfaces is not limited to gas-crystal systems. Incorporation of zeolite membranes with amorphous polymer membranes is of interest for gas separation. These hybrid systems combine molecular sieving properties and entropic selectivities of zeolites with separation performance of polymeric membranes. Hofmann and coworkers studied the interfacial region between zeolite and polymer that is of decisive importance for the overall separation characteristics of composite membrane material.[21] Their work showed that a good adhesive contact between zeolite and polymer resulted in a significant decrease in penetrant mobility (diffusivity).

Studies of complete membranes have been relatively few and more recent. Takaba et al.[18] studied permeation of iso- and *n*-butane through a 4 nm thick silicalite membrane in the direction of straight channels, showing that the membrane can separate the two isomers. Martin et al.[19] studied the diffusion of methane through silicalite membranes ranging in thickness from 2 to 16 nm, with diffusion oriented along the straight channels. The results of Martin et al.[19] showed that the surface resistance increased as the membrane became thicker, in contradiction to initial expectations that the resistances at the surface were constant beyond the first few angstroms inside the surface.

This observation was originally interpreted as an artifact, but our previous simulations[22] showed that the effect was apparent even at different crystal orientations and for thicker crystals. Although the surface resistance eventually must approach a limiting value, the membrane thickness before this approach is surprising. The range of the thickness when this limit is approached is what we refer to as the "range" effect. From individual simulations of exit and entrance zones, we have explored the range over which the resistances increase asymptotically to a constant value. Exploring the parametric sensitivity of this range effect motivates the current manuscript.

In our previous work,[22] we studied the diffusion process of methane in a silicalite SCM using the Dual Control Volume-Grand Canonical Molecular Dynamics (DCV-GCMD) method, as did Martin et al.[19] The objective of the present work is to apply the same methodology to understand the variation in dynamics dictating the diffusion of molecules through the SCM along the (*z*-) direction, which is the actual operation direction in practice, with the nature of permeants. For this purpose three spherical molecules have been selected: CH_4, Ar, and CF_4. This selection enables the study of a range of molecular diameters and interaction energies. Additionally, the parameters for permeant-crystal interaction size and well depth, as well as molecular weight, were varied artificially in the manner of a factorial design to check for the significance of these factors and their cross-interactions during their adsorption from gas phase into the silicalite.

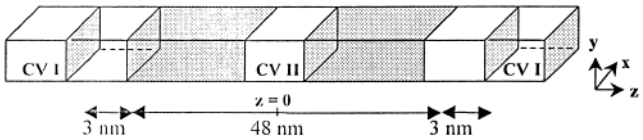

Figure 1. Schematic (not to scale) of DCV-GCMD simulation box. The shaded area is filled with zeolite. Both sections of CV I at the ends are connected with each other through the periodic boundary conditions. The box is symmetric with respect to the central plane at $z = 0$.

2. DCV-GCMD Simulations

The basis for DCV-GCMD is to carry out grand canonical Monte Carlo (GCMC) insertions and deletions in two control volumes (CVs) placed inside the simulation box of a molecular dynamics simulation (MD), to establish a steady-state chemical potential gradient between these CVs.[12,23,24]

The simulations were performed along the (*z*-) direction of the membrane that corresponds to the [0 0 1] axis of the silicalite unit cell.[25] The simulation box in Figure 1 consists of two mirror-image boxes, symmetric with respect to the center plane in order to satisfy the periodic boundary condition in the permeating (*z*-) direction. The box has a cross-sectional area of 4 nm × 4 nm (2 unit cells × 2 unit cells) in the (*x*-) and (*y*-) directions. Each symmetric box has three regions: two control volumes CV I and CV II, positioned outside and in the middle of the membrane, respectively, for individual surface studies and a transport region between them. The thickness of the crystal inside the transport region (the shaded area) was set as multiples of the silicalite unit-cell length in the [0 0 1] direction. For the intracrystalline diffusion simulations, both CVs are filled with silicalite, and for the entrance/exit simulations, only CV II is filled. For total membrane simulations, both CVs are placed 3 nm away from the corresponding membrane surface to avoid undesired interactions with newly inserted molecules and molecules already adsorbed on the surface. During the simulations, the length of each CV was set to 16 nm, except when CV I was located inside the bulk gas phase. In this latter case the length of CV I was set to 150 nm.

The chemical potential difference between the CV I and CV II regions acts as the driving force for diffusion of the methane molecules. Therefore the chemical potentials in the two CVs must be maintained at some fixed values, which are in equilibrium with two bulk phases, each at a fixed gas pressure. To keep the densities constant in the CVs, the insertion and destruction algorithms of the GCMC method are implemented. The chemical potentials in the CVs are imposed by the pressure of the gas molecules, under the ideal gas assumption. The details of the procedure can be found elsewhere.[26]

When a particle is inserted into a CV, it is assigned a random thermal velocity selected from a Gaussian distribution at the given temperature. A streaming velocity was added to the thermal velocity of all the newly inserted methane molecules that were located within each CV, to maintain continuous and monotonic chemical potentials at the boundaries between the CVs and the transport region.[27] Adding streaming velocities was also necessary to eliminate undesired transport resistances at the interfaces between the transport region and control vol-

TABLE 1: Lennard-Jones Potential Parameters for CH_4, Ar, and CF_4 in Silicalite

	σ_{gg} (Å)	ϵ_{gg} (K)	σ_{go} (Å)	ϵ_{go} (K)	ref
CH_4	3.73	148	3.64	96.5	[29]
Ar	3.42	124	3.17	95.61	[37]
CF_4	4.66	134	3.73	109.6	[38]
CH_4*	3.73	148	3.214	133.3	[30]

umes.[28] The magnitude of the streaming velocity was set by a trial and error procedure such that the chemical potential be constant inside the control volumes and no discontinuity occur at the boundaries of the control volumes. The final increment in velocity of the *z*-component was roughly 10% of the thermal velocity within the cell boundaries.

Molecules spontaneously move along the chemical potential gradient through a conventional molecular dynamics algorithm, and a nonequilibrium steady state is obtained in the transport region. MD-time steps of 5 fs for Ar and CH_4, and 10 fs for CF_4 were adopted. Isothermal conditions were maintained by rescaling the velocity in all three directions after each MD step.[27] To maintain the correct density and chemical potentials in the CVs, the ratio of GCMC equilibration to MD steps was set at 1:100 for CV I, and varied between 1:200 and 1:500 for CV II. The maximum number of insertion/deletion attempts at each GCMC equilibration was set to 20 inside the gas phase, and 750 inside the crystal. Simulations were started with an empty box, and fluxes through the membrane were measured at five equidistant planes perpendicular to the direction of flow. After each 1500 ns (1.5 μs), the fluxes were checked at each plane, and the procedure was continued, depending on the crystal thickness, until a steady-state flow was obtained through all planes. Once the steady state was established, the fluxes through the planes were sampled for at least 3000 ns (3.0 μs), averaging after each 1500 ns.

To obtain the chemical potential profile, the membrane was divided into bins and the excess chemical potential within these bins was calculated by the test particle insertion method of Widom.[26]

In the present work, the spherical Lennard-Jones (LJ) potential model was used for the gas molecules and permeant-zeolite interactions. The silicalite framework was assumed to be rigid. The silicon atoms in the zeolite were neglected and, to account for their absence, modified oxygen interaction parameters were used. All interactions between existing molecules were described by the 12−6 LJ-potential given as

$$\phi_{ij} = 4\epsilon_{ij}\left[\left(\frac{\sigma_{ij}}{r}\right)^{12} - \left(\frac{\sigma_{ij}}{r}\right)^{6}\right] \tag{1}$$

where r is the distance between interaction centers, i and j, which are allotted among permeating gas molecules or oxygen atoms, and σ_{ij} and ϵ_{ij} are potential parameters for the pair i and j. The pure LJ parameters for the permeants, and those for the permeant-zeolite interactions, are listed in Table 1. The table includes a second LJ-interaction parameter set for methane, labeled as CH_4*, which was used in the parameter analysis. Note that both sets of parameters for CH_4 yield similar heat of adsorption (−18 kJ/mol at 298 K) and equilibrium properties, but have significantly different size and energy parameters with respect to each other.[29,30] The cutoff distance for calculations of the intermolecular interactions was set at 1.0 nm, and the long-range correction was not applied. The potential and the force vector were evaluated using the pretabulation method, which uses the symmetry property of the 1/8th zeolite unit cell.[31,32]

3. Results

To evaluate the variations in individual contributions of adsorption, intracrystalline transport, and desorption steps into the diffusion process, the simulations for each set of operating conditions were broken down into three regions: entrance, intracrystalline, and exit simulations. The flux during an intracrystalline simulation is given by

$$j = -\frac{D_t}{RT}\frac{\mathrm{d}P}{\mathrm{d}z} \tag{2}$$

where D_t is uncorrected intracrystalline transport diffusivity, and P is the pressure in equilibrium with a given concentration inside the crystal. Since the transport diffusivities vary with concentration,[3] the corrected diffusivities D_o were calculated using Darken's correction factor[10] (δ) to account for the effect of operating pressures in the CVs

$$D_o = D_t\frac{d\ln q}{d\ln P} = D_t\frac{1}{\delta} \tag{3}$$

where q is the concentration in the micropores. Then eq 2 becomes

$$j = -\frac{\delta D_o}{RT}\frac{\Delta P}{\Delta z} = -\frac{\delta D_o}{RT}\frac{\Delta P}{L} \tag{4}$$

where ΔP is the difference between the pressures in CV I and CV II that sets the chemical potential gradient over a crystal thickness L. Then the flux can be rewritten in terms of a diffusive resistance, which is independent of the concentration, as:

$$j = -\frac{\delta}{R_{intra}}\frac{\Delta P}{RT} \tag{5}$$

The accuracy of Darken's approximation, which assumes the corrected diffusivity does not vary with concentrations, was investigated by Skoulidas and Sholl.[33,34] The authors showed that the approximation is not valid in general. While Darken's approximation holds for CH_4 and Ar molecules in silicalite, a decrease in corrected diffusivity of CF_4 was observed as the concentration increased beyond 2 molecules per unit cell. In our simulations, the maximum loading of CF_4 remained around 1.25 molecules per unit cell, therefore we assumed that the Darken's approximation was valid for all three molecules studied.

The total resistance acting on a complete membrane may be calculated as the sum of individual contributions,

$$R_{tot} = R_{ads} + R_{intra} + R_{des} \tag{6}$$

where R_{ads} and R_{des} are the resistances to adsorption and desorption. The overall flux is related to the total pressure of the system by

$$J_o = -\frac{\delta}{R_{tot}}\frac{\Delta P}{RT} \tag{7}$$

Then the overall diffusion coefficient as measured experimentally can be represented as

$$D_{exp} = \frac{\delta L}{\left[R_{ads} + \frac{L_{intra}}{D_o} + R_{des}\right]} \tag{8}$$

One question addressed by the simulations is whether the surface

resistances are substantial enough to alter the value of D_{exp}, or whether $D_{exp} \sim D_t$ is a reasonable approximation. In our previous work[22] we observed that the fugacity became relatively flat at short distances from the surface. Hence, L_{intra} was set equal to L, the distance between the crystal surface and CV II, to simplify the analysis.

3.1. Diffusion of CH_4, Ar and CF_4. *3.1.1. Intracrystalline Resistance.* Intracrystalline simulations were conducted by creating a pressure (fugacity) gradient inside the crystal as described in the previous section. These simulations have revealed the isolated contribution of the intracrystalline transport.

Once the flux was obtained as the result of simulations, corrected diffusivities were calculated from eqs 3 and 4. In the presence of a virial isotherm equation, as in the case for CH_4,[10,22] q can be related to P after some manipulations. As such isotherms were not available for Ar and CF_4, an alternative method was used to calculate the corrected diffusion, considering the isothermal diffusion of gas molecules through the crystal.[35] Then eq 2 can be written in terms of the chemical potential gradient

$$j = -\frac{D_o c(z)}{RT}\frac{d\mu}{dz} \tag{9}$$

where $c(z)$ is the local concentration. With the assumption that $d\mu/dx$ can be replaced by $\Delta\mu/\Delta x$, and $c(z)$ with c_{avg}, which is the average concentration inside the transport region (between CVI and CVII), eq 9 becomes

$$j = -\frac{D_o c_{avg}}{RT}\frac{\Delta\mu}{L} \tag{10}$$

Once the transport and corrected diffusivities are known from the intracrystalline simulations, Darken's correction factor can be obtained to calculate the corrected diffusivities from entrance and exit simulations.

To check the compatibility of the two methods mentioned above, a corrected diffusivity (D_o) of CH_4 was calculated at 298 K using both of the methods; the methods yielded 2.24×10^{-5} cm^2/s and 2.20×10^{-5} cm^2/s, respectively, for an average loading of 1.8 molecules/unit cell.

As result of simulations at different loadings, the average corrected self-diffusivity of Ar was calculated as 2.61×10^{-5} cm^2/s. Because the corrected diffusivity of CF_4 decreases with increasing loading, its average value was determined as 0.69×10^{-5} cm^2/s from the simulations performed below a loading of 2 molecules per unit cell. Figure 2 shows corrected diffusivities for the permeants in comparison with the equilibrium MD results of Skoulidas and Sholl.[34] The diffusivity of CF_4, which is the larger molecule, is the lowest, and the diffusivity of Ar is the highest. Note that this ordering depends strongly on the selection of LJ parameters for the permeants; the figure includes the diffusivity for CH_4*, which was calculated with an alternative set of parameters. The sensitivity of diffusivity and mass transfer resistance to the potential parameters is investigated later in this paper.

3.1.2. Entrance and Exit Resistances. In this part of this work, the entrance effect has been studied to reveal the change in the entrance resistances acting on the permeants. In these simulations CV II has been filled with crystal cells and the adsorption steps have been simulated by setting inlet and outlet pressures. The "pressures" in the CVs interior to the crystal were determined by the pressure of the ideal gas being equilibrated in the GCMC sampling.

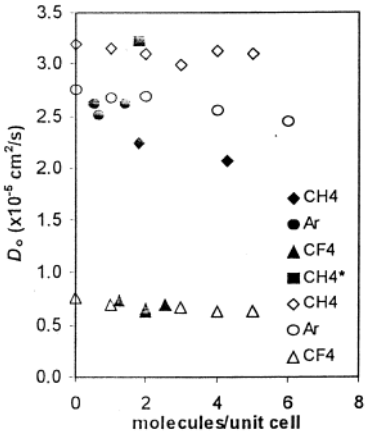

Figure 2. Corrected diffusivities for the permeants (this work, solid marks) in comparison with the equilibrium MD results of Skoulidas and Sholl[34] (open marks). The same LJ parameters were used in both works for all permeants except CH_4, which was also simulated with an alternative set of LJ parameters (CH_4) in addition to the one used by Skoulidas and Sholl (CH_4*). (See Table 1)

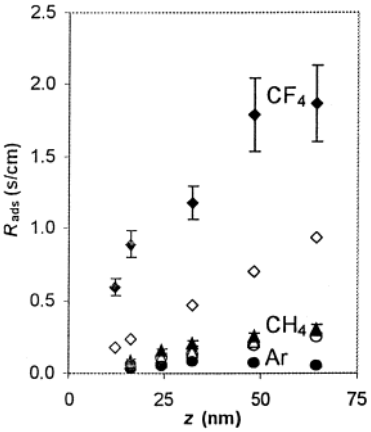

Figure 3. Change of mass-transfer resistances at the entrance with crystal thickness for CH_4, Ar, and CF_4. The open marks show intracrystalline resistance for the permeants corresponding to the shape of solid marks. The same representation applies to the rest of the figures. Note the overlapping marks for intracrystal resistance of CH_4 and Ar due to the scale.

Entrance simulations combine the adsorption and intracrystalline transport effects. The total resistance acting on this system is the sum of adsorption and intra-crystalline resistance:

$$R_{ads} = R_{tot} - R_{intra} = R_{tot} - \frac{L_{intra}}{D_{intra}} \tag{11}$$

The pressures of CV I and CV II are set to 1 and 0 bar, respectively, to establish the fugacity gradient. The thickness of the membrane was varied between 16 and 64 nm to observe the variation on the surface resistance. As shown in Figure 3, the mass-transfer resistance acting on CF_4, which is the larger molecule, is the strongest, whereas the mass-transfer resistance for Ar is the weakest. In our previous study,[22] we showed that for thinner crystals the adsorption resistance for CH_4 increases monotonically with crystal thickness. A similar behavior was also observed in the current study for Ar, and CF_4. But the increase in the resistance for Ar approaches to an asymptotic beyond a short distance. This asymptotic behavior is expected for each molecule beyond a certain thickness. Molecules with high diffusivity and low surface resistance approach the asymptotic value at relatively short distances.

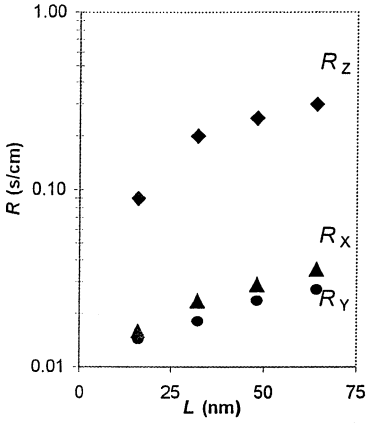

Figure 4. Comparison of the magnitude and range of mass-transfer resistance of CH_4 at the entrance for each of the three crystal orientations on a semilog scale.

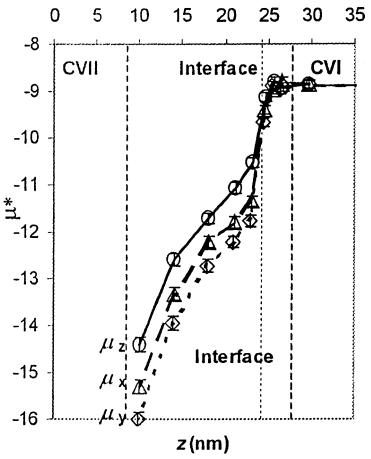

Figure 5. Chemical potential gradient of CH_4 in each of the three crystal orientations.

We also compared the range and magnitude of entrance resistance in all three diffusional directions by changing the orientation of the crystal. Figure 4 shows that the range of the surface resistances is similar in each direction although their magnitudes are different due to directionally varying diffusivities. Similarly, the chemical potential gradient in all directions are qualitatively identical as shown in Figure 5. These observations show that the range of the surface resistance is a function of molecular characteristics, that is, gas-crystal interaction energy and size, and independent of the magnitude of diffusivity and direction of diffusion.

In our previous work we had speculated that the range of the mass-transfer resistance to adsorption for methane would be around 150 nm. To further investigate the long-range changes in the entrance resistance, the membrane thickness was increased to 128 nm for CH_4. The result, as shown in Figure 6, indicates that at this thickness the surface resistance is still far from its final value, thus its range is longer than initially expected. Also at this thickness intracrystalline mass-transfer resistance reaches to the value of entrance resistance; beyond this thickness intracrystalline resistance will exceed surface resistance. This observation shows that the argument of Kocirik et al.,[5] who argued that surface resistance could exceed intracrystalline resistance by several orders of magnitude for crystals smaller than 1 μm, is not valid for spherical permeants diffusing through silicalite membranes. If the variation of mass-transfer resistances is extrapolated to a crystal of 1 μm thickness, the contribution of surface resistance to overall mass-transfer resistance can be

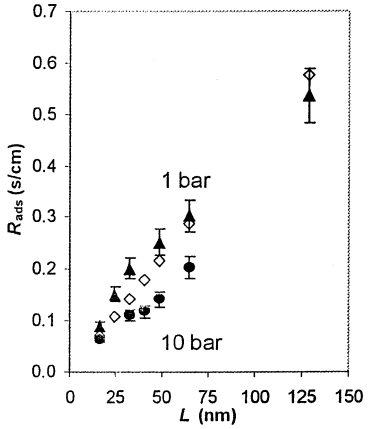

Figure 6. Variation in adsorption resistance to CH_4 diffusion at 1 and 10 bar.

estimated approximately as 1−2% for Ar and 15−20% for CH_4. For CF_4 we were unable to estimate the contribution since the range to asymptote was too far an extrapolation, which indicates that it is larger than that for CH_4. The contribution of surface resistance to overall resistance varies also according to the crystal orientation: we estimated that along the (*y*-) direction, in which the diffusion is 10 times faster than in the (*z*-) direction, the contribution at a thickness of 1 μm would be 10% for CH_4. This estimation is based on the result of simulations in the (*y*-) direction showing that the magnitude of intracrystalline resistance catches up to that of the entrance resistance at 80 nm, in contrast to 128 nm in the (*z*-) direction, and beyond that thickness it exceeds the entrance resistance.

Furthermore, to check the role of permeant concentration in the crystal on surface resistance, simulations for CH_4 were run by setting the inlet pressure at 10 bar. The comparison of adsorption resistances at 1 and 10 bar in Figure 6 showed that the magnitude of surface resistance was lower at 10 bar. This decrease can be attributed to increased frequency of contacts among molecules adsorbed inside the crystal channels, due to higher permeant loading. Considering both the entrance end exit resistances arise due to the discontinuity of the potential field created by the gas/crystal interface, the decrease in the surface resistance at higher loadings corroborates with the work of Arya et al.[17] They studied the exit resistance, and argued that surface resistance at the exit is more important at lower loadings since the escape of a molecule is unaffected by the presence of the other molecules, and at higher loadings, the local clustering of molecules caused a considerable reduction of the exit barrier.

When this observation is combined with the previous results of CF_4 and Ar diffusion, we conclude that the range of the surface resistance is primarily a function of molecular size. Noting that size determines the mean-free-path of gas molecules in the crystal, we may speculate that dissipation of the surface resistance is impeded by reduction in the mean-free-path. As the molecular size increases, the mean-free-path decreases inside the zeolite channels, reducing the frequency of contact among the adsorbed gas molecules, and thus reducing the momentum transfer along the fugacity gradient. In the presence of large simulated fugacity gradients, molecules must conduct momentum from regions of high fugacity to low by contacting each other. To be specific, consider molecules near the entrance to the crystal. When the fugacity gradient is large, travel toward high fugacity is extremely likely to bring a large impulse in the opposite direction. The impacted molecules come crashing back toward the interior of the crystal, dissipating their energy through contacts with the solid, and occasionally with other gas atoms.

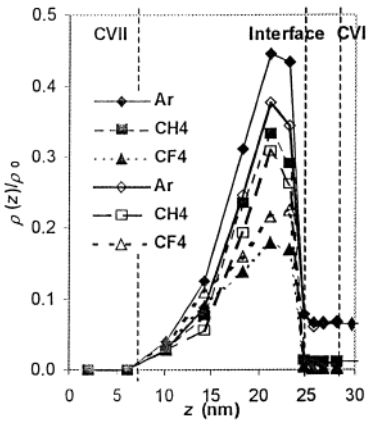

Figure 7. Concentration profiles of Ar, CH_4, and CF_4 at 0.26 bar (solid marks) and 0.55 bar (open marks). The profiles are normalized for each species by the equilibrium concentration inside the crystal at corresponding pressures.

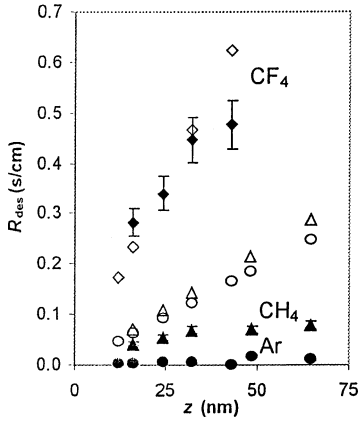

Figure 8. Change of mass-transfer resistances at the exit with crystal thickness.

The succeeding layers away from the high gradient moderate this likelihood until the only significant effect is the intracrystalline gradient.

Note that the fugacity gradient reflects the concentration gradient of the permeants. Figure 7 exhibits normalized concentration profiles of all three gas molecules through a 16 nm-crystal entrance at 298 K: The profiles were calculated at 0.26 and 0.55 bar inlet pressures, and normalized with respect to equilibrium concentrations of permeants at the corresponding pressure. Comparison of these profiles shows that their steepness was proportional to diffusivities of molecules: that is, the fastest diffusing Ar had the higher gradient, and so on. Furthermore, the concentration gradients of Ar and CH_4 decreased with pressure, while the gradient of CF_4 was higher at the higher pressure. Qualitatively speaking, the slope of the normalized concentration profile reflects the range of surface resistance.

Exit simulations combine the exit and intracrystalline transport effects. The total resistance acting on this system is the sum of desorption and intra-crystalline resistance:

$$R_{des} = R_{tot} - R_{intra} = R_{tot} - \frac{L_{intra}}{D_{intra}} \qquad (12)$$

Simulations of exit resistances were run again at 298 K by setting the pressures in CV I and CV II to 0 and 1 bar, respectively, with thickness of the membrane varying between 16 and 64 nm. As shown in Figure 8, the mass-transfer resistances acting on permeants at the exit are qualitatively similar to those at the entrance.

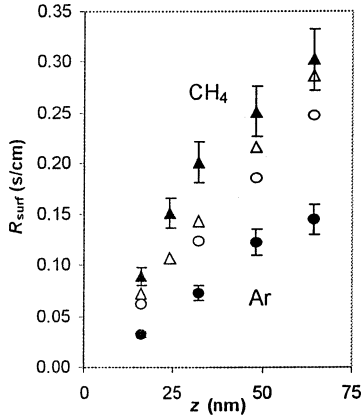

Figure 9. Change of mass-transfer resistances with membrane thickness for Ar and CH_4.

Individual simulations for exit and entrance effects indicated that the resistance to adsorption is stronger than that to desorption for each penetrant. Results of the simulations indicated that the resistance for CF_4 is the strongest in either case due to its large size, as expected based on the adsorption resistance, and the resistance for Ar is the weakest. Although Ar and CH_4 have similar penetrant-crystal interaction energies, the smaller size of Ar leads to the difference observed. Similar to adsorption resistances, the desorption resistance for Ar levels off in a much shorter distance than that of CH_4; for CF_4, the simulated membrane thickness was insufficient to observe asymptotic behavior.

3.1.3. Membrane Simulation. The contribution of surface resistance with increasing membrane thickness has been compared for Ar and CH_4 by varying the thickness from 16 to 64 nm. The temperature of the system was kept at 298 K, and the inlet pressure was set to 1 bar. Simulation runs were carried out for the outlet pressure at vacuum. Surface resistance for the membrane was calculated by subtracting intracrystalline resistance from total resistance:

$$R_{surf} = R_{tot} - R_{intra} \qquad (13)$$

The variation of surface resistances is shown in Figure 9. Note that the surface resistances obtained from membrane simulations are slightly lower than the sum of adsorption and desorption resistance calculated from independent simulations, since the thickness of the membrane was not large enough to decouple resistances at the entrance and exit.[22] The surface resistance for Ar again shows a similar trend to that for CH_4, with smaller magnitudes as in the cases of entrance end exit simulations.

3.2. Parametric Sensitivity Analysis. In this part of the work, a parametric sensitivity analysis was carried out using Yates' factorial design algorithm[36] by artificially varying the parameters for permeant-crystal interaction size and well-depth, as well as molecular weight, in the manner of a factorial design to check for the significance of these factors and their cross-interactions during their adsorption from gas phase into the silicalite. The purpose of the factorial design is to establish a standard linear model to analyze the influence of variables by performing two (computer) experiments at two different levels of each variable. In this way, the influences of the variables and their relevant interactions can be analyzed with the minimum number of experiments. To perform Yates' 2^3-factorial analysis, the high and low values of the LJ parameters were set by combining the LJ parameters of CH_4 and CH_4*. These two molecules will be labeled as M_1 and M_2, respectively, in this part of the work. Cross-interactions were studied by the combination of these

TABLE 2: Parameter Sets and Corresponding 2^3-design for the Sensitivity Analysis of Permeant Flux. *S*, *E*, and *W* Are the Identifiers for the Factors Diameter, Energy, and Weight, Respectively. The '0's and '1's Represent the Low and High Values of the Parameters

	$\sigma(A)$ *S*	$\epsilon/k(K)$ *E*	*MW W*	2^3			effect
M_0	3.214	96.5	16	0	0	0	Avg
M_1	3.640	96.5	16	1	0	0	S
M_2	3.214	133.5	16	0	1	0	E
M_3	3.640	133.3	16	1	1	0	SE
M_{0w}	3.214	96.5	32	0	0	1	W
M_{1w}	3.640	96.5	32	1	0	1	SW
M_{2w}	3.214	133.5	32	0	1	1	EW
M_{3w}	3.640	133.3	32	1	1	1	SEW

TABLE 3: Permeant Corrected Diffusivities from the Intracrystalline Simulations and Estimated Effects from Yates' Parametric Analysis. The Columns 'Est.' Show the Estimated Effect of Each Parameter and Their Interactions on the Value of Diffusivity

	298 K		330 K		
	D_o (10^{-5} cm^2/s)	est.	D_o (10^{-5} cm^2/s)	est.	effect
M_0	4.44	2.53	4.54	3.07	Avg
M_1	2.28	−1.31	2.87	−1.70	S
M_2	3.22	−0.81	3.71	−0.68	E
M_3	2.03	0.45	2.43	0.20	SE
M_{0w}	3.2	−0.92	4.18	−0.63	W
M_{1w}	1.83	0.36	2.06	−0.22	SW
M_{2w}	1.9	−0.07	3.26	−0.04	EW
M_{3w}	1.37	−0.03	1.54	0.00	SEW

parameters. The weight effect is probed by doubling the molecular weight. The parameter list of the investigated cases and corresponding 2^3-designs are given in Table 2. Hence, the linear model to estimate the contribution of each factor becomes

$$Y = e_0 + e_1S + e_2E + e_3W + e_{12}SE + e_{13}SW + e_{23}EW + e_{123}SEW \quad (14)$$

Where '*Y*' is the estimated value of the property such as the flux, diffusivity, or surface resistance, and *S*, *E*, and *W* are the factors identifying the parameters cited above. The coefficients 'e_i' are that of the orthogonal design matrix given in the table. When all the factors are at their lower values, the value of '*Y*' corresponds to the average value of the measured property. Then by varying the parameters according to Yates' algorithm, the significance of each parameter on the value of measured properties is evaluated. The simulations for entrance and intracrystalline diffusion were run at 298 and 330 K. The temperature has not been incorporated into the 2^N design. First, the temperature was not a molecular characteristic. Second, temperature and interaction energy would always be coupled by counter-balancing each other, that is, a decrease in energy would show a similar effect to an increase in temperature, and vice versa.

Throughout the simulations, the thickness of the transport region inside the crystal in each case was kept at 16 nm, and the pressures at CV I and CV II were set to 1 bar and vacuum, respectively. The fluxes obtained from these simulations were used to calculate the diffusivities, which were then corrected using Darken's factor.

The parametric sensitivity analysis is first conducted for intracrystalline diffusion. Corrected diffusivities and the corresponding Yates analysis are listed in Table 3. Results indicate that size and energy obviously dictate the magnitude of diffusivity: diffusivity is higher when gas-crystal interaction size and well depth are smaller, as the permeating molecules move freely through the crystal. When these two parameters have a higher value the molecules get "stickier", and move much more slowly inside the crystal; thus the diffusivity decreases. The interaction of molecular weight with size shows an increasing effect on diffusivity at low temperature. In contrast, the interaction between weight and size has an opposite effect at high temperature. This behavior shows a tradeoff between size and weight factors: at low temperature, larger interaction diameter inhibits diffusion, but as the molecules get heavier, they move more easily through pore channels due to increased momentum. At high temperature, pore walls become "softer" and the increased size has less of an inhibiting effect, therefore the weight's only contribution is slowing the diffusion of molecules down.

TABLE 4: Permeant Fluxes and Corrected Diffusivities from the Entrance Simulations and Estimated Effects from Yates' Parametric Analysis

	298 K		330 K		
	D_o (10^{-5} cm^2/s)	est.	D_o (10^{-5} cm^2/s)	est.	effect
M_0	3.04	1.33	3.18	1.66	Avg
M_1	0.84	−1.38	1.14	−1.74	S
M_2	1.71	−0.77	2.41	−0.61	E
M_3	0.64	0.52	0.69	0.14	SE
M_{0w}	2.28	−0.46	2.64	−0.38	W
M_{1w}	0.68	0.26	0.91	0.14	SW
M_{2w}	1.03	0.00	1.91	0.00	EW
M_{3w}	0.39	−0.04	0.43	−0.02	SEW

TABLE 5: Total and Surface (Adsorption) Resistances for the Permeants at the Entrance into the Crystal, with Sensitivity Analysis of Effects on % Contribution of Surface Resistances

	298 K				330 K				
	R_{tot} (s/ m)	R_{ads} (s/ m)	R_{ads}/R_{tot} %	est.	R_{tot} (s/ m)	R_{ads} (s/ m)	R_{ads}/R_{tot} %	est.	effect
M_0	5.26	1.66	31.5	52.41	5.03	1.51	30.0	50.78	Avg
M_1	19.03	12.01	63.1	28.23	14.07	8.50	60.4	29.80	S
M_2	9.36	4.39	46.9	11.53	6.64	2.33	35.1	10.05	E
M_3	25.03	17.15	68.5	-4.68	23.28	16.69	71.7	5.20	SE
M_{0w}	7.03	2.03	28.9	-0.17	6.06	2.24	36.9	2.95	W
M_{1w}	23.67	14.93	63.1	1.63	17.54	9.77	55.7	-3.70	SW
M_{2w}	15.57	7.15	45.9	1.13	8.38	3.48	41.5	1.85	EW
M_{3w}	40.89	29.22	71.4	0.33	41.32	30.93	74.9	2.10	SEW

The effect of the LJ parameters becomes more significant during the entrance of the molecules into the silicalite crystal, as shown in Table 4. As an example, the diffusivity of M_1 is 28% of that of M_0 at the entrance, in contrast to 51% at the intracrystalline diffusion. This trend is valid for both light and heavy molecules at both temperatures.

Next, the effects of parameters at the entrance are compared in terms of mass-transfer resistances. Since the only surface resistance present in these simulations is adsorption resistance, the effective total resistance is the sum of adsorption and intracrystalline resistances. The comparison of permeants in terms of total and adsorption resistances along with percent contribution of adsorption resistance is shown in Table 5. The table also includes a sensitivity analysis in terms of contributions. The results show that size has a dramatic effect on adsorption resistance, as well as on its contribution to total resistance. The effect of energy is also substantial, but relative to a lesser extent. The reason for the increase in the adsorption resistance due to size and energy is that the penetration of molecules through pores at the crystal surface is inhibited as they become larger and "stickier". The weight of the molecules and the temperature do not alter this general behavior.

These simulations showed that for molecules with similar equilibrium properties, such as heat of adsorption or equilibrium

concentration, the dynamic properties, such as diffusivities, can be significantly different.

4. Conclusion

In this work we showed that the magnitude and range of surface resistance in zeolite membranes depend on the permeant-crystal interaction size and energy of the permeants. Simulation results indicated that the size effect is more important to determine the magnitude of surface resistances compared to the energy effect, as a small difference in size causes large differences in the magnitude of resistances. Furthermore the range of the surface resistance is primarily a function of molecular size: For smaller molecules the range of surface resistances becomes shorter than that for larger molecules. This behavior is determined by the mean-free-path of gas molecules in the crystal: As the molecular size increases, the mean-free-path decreases inside the zeolite channels, which reduces the interaction among the adsorbed gas molecules.

We observed that as the crystal thickness increases above 1 μm, intracrystalline mass-transfer resistance exceeds surface resistance in contradiction to Kocirik et al.[5] The contribution of surface resistance to overall mass-transfer resistance when extrapolated to a crystal of 1 μm thickness would be approximately 15−20% for CH_4 and 1−2% for Ar, indicating that surface resistance becomes more important for slow-diffusing molecules. Additionally, the comparison of adsorption resistances at 1 and 10 bar showed that the magnitude of surface resistance decreases as the pressure increases. This decrease can be explained by an increased frequency of contacts among adsorbed molecules due to higher loading. This finding agrees with the work of Arya et al.,[17] where they argued that surface resistance at the exit is more important at lower loadings since the escape of a molecule is unaffected by the presence of the other molecules, and at higher loadings, the exit barrier decreases as a result of the local clustering of molecules. Thus, the magnitude of surface resistance is governed by the extent of interaction among adsorbed gas molecules inside the crystal: as the concentration inside the crystal increases or the permeant-crystal interaction size decreases, the occurrence of contacts among the permeants increases resulting in a decrease in surface resistance.

The parametric sensitivity analysis showed that the LJ gas-crystal interaction parameters are crucial to predict the diffusivities of the molecules that penetrate silicalite crystal. Although different sets of parameters yield similar equilibrium concentration values in adsorption studies, the surface resistance varies drastically with variations in these parameters during the diffusion process. The study, thus, provides a basis to better understand the contribution of the surface barriers during diffusion through thin crystals membranes.

Acknowledgment. This work was supported in part by the National Science Foundation. (Grant No. CTS-9725256)

References and Notes

(1) Shah, D. B.; Ruthven, D. M. *AIChE J.* **1977**, *23*, 804−809.

(2) Shah, D. B.; Hayhurst, D. T.; Evanina, G.; Guo, C. J. *AIChE J.* **1988**, *34*, 1713−1717.

(3) Karger, J.; Ruthven, D. M. *Zeolites* **1989**, *9*, 267−281.

(4) Ruthven, D. M. *Stud. Surf. Sci. Catal.* **1995**, *97*, 223−234.

(5) Kocirik, M.; Struve, P.; Fiedler, K.; Bulow, M. *J. Chem. Soc., Faraday Trans. 1* **1988**, *88*, 3001.

(6) Ford, D. M.; Glandt, E. D. *J. Membr. Sci.* **1995**, *107*, 47−57.

(7) Barrer, R. M. *Langmuir* **1987**, *3*, 309.

(8) Karger, J.; Ruthven, D. M. *Diffusion in Zeolites and Other Microporous Solids*; Wiley: New York, 1992.

(9) Sun, M. S.; Talu, O.; Shah, D. B. *AIChE J.* **1996**, *42*, 3001−3007.

(10) Talu, O.; Sun, M. A.; Shah, D. B. *AIChE J.* **1998**, *44*, 681−694.

(11) Maginn, E. J.; Snurr, R. Q.; Bell, A. T.; Theodorou, D. N. *Stud. in Surf. Sci. and Catal.* **1997**, *105*, 1851−1858.

(12) Heffelfinger, G. S.; van Swol, F. *J. Chem. Phys.* **1994**, *100*, 7548−7552.

(13) Nicholas, J. B.; Trow, F. R.; Mertz, J. E.; Hopfinger, A. *J. Phys. Chem.* **1993**, *97*, 4149−4163.

(14) Hernandez, E.; Catlow, C. R. A. *Molecular-Dynamics Simulations of n-Butane and n-Hexane Diffusion in Silicalite*, Proceedings of the Royal Society of London Series A, 1995; London.

(15) Vingé-Maeder, F.; El Amrani, S.; Gélin, P. *J. Catal.* **1992**, *134*, 536−541.

(16) Skoulidas, A. I.; Sholl, D. S. *J. Chem. Phys.* **2000**, *113*, 4379−4387.

(17) Arya, G.; Maginn, E. J.; Chang, H.-C. *J. Phys. Chem. B* **2001**, *105*, 2725.

(18) Takaba, H.; Koshita, R.; Muzkami, M. *J. of Membr. Sci.* **1997**, *134*, 127−139.

(19) Martin, M. G.; Thompson, A. P.; Nenoff, T. M. *J. Chem. Phys.* **2001**, *114*, 7174−7181.

(20) Bowen, T. C.; Falconer, J. L.; Noble, R. D.; Skoulidas, A. I.; Sholl, D. S. *Ind. Eng. Chem.* **2002**, *41*, 1641−1650.

(21) Hofmann, D.; Fritz, L.; Ulbrich, J.; Schepers, C.; Böhning, M. *Macromol. Theory Simul.* **2000**, *9*, 293.

(22) Ahunbay, M. G.; Elliott, J. R.; Talu, O. *J. Phys. Chem. B* **2002**, *116*, 5163−5168.

(23) Thompson, A. P.; Ford, D. M.; Heffelfinger, G. S. *J. Chem. Phys.* **1998**, *109*, 6406.

(24) MacElroy, J. M. D. *J. Chem. Phys.* **1994**, *101*, 5724.

(25) Meier, W. M.; Olson, D. H. *Atlas of Structure Types*; IZA Special Publications: Guildford, 1978.

(26) Frenkel, D.; Smit, B. *Understanding Molecular Simulation: from Algorithms to Applications*; Academic Press: San Diego, 1996.

(27) Xu, L.; Tsotsis, T. T.; Sahimi, M. *J. Chem. Phys.* **1999**, *111*, 3252−3264.

(28) Arya, G.; Chang, H.-C.; Maginn, E. J. *J. Chem. Phys.* **2001**, *115*, 8112−8124.

(29) Smit, B.; Siepmann, J. I. *J. Phys. Chem.* **1994**, *98*, 8442−8452.

(30) Goodbody, S. J.; Watanabe, K.; MacGowan, D.; Walton, J. P. R. B.; Quirke, J. *J. Chem. Soc., Faraday Trans* **1991**, *87*, 1951−1958.

(31) June, R. L.; Bell, A. T.; Theodorou, D. N. *J. Phys. Chem.* **1990**, *94*, 8232.

(32) Talu, O.; Myers, A. L. Molecular Diffusion in a Single Zeolite Crystal, *Fundamentals of Adsorption*; Kluwer, 1996.

(33) Skoulidas, A. I.; Sholl, D. S. *J. Phys. Chem. B* **2001**, *105*, 3151−3154.

(34) Skoulidas, A. I.; Sholl, D. S. *J. Phys. Chem. B* **2002**, *106*, 5058−5067.

(35) Mason, E. A.; Lonsdale, H. K. *J. Membr. Sci.* **1990**, *51*, 1−81.

(36) Box, G. E. P.; Hunter, W. G.; Hunter, J. S. *Statistics for experimenters: an introduction to design, data analysis, and model building*; Wiley: New York, 1978.

(37) Clark, L. A.; Gupta, A.; Snurr, R. Q. *J. Phys. Chem. B* **1998**, *102*, 6720−6731.

(38) Heuchel, M.; Snurr, R. Q.; Buss, E. *Langmuir* **1997**, *13*, 6795−6804.